

Transmissive RIS for 6G Communications: Design, Prototyping, and Experimental Demonstrations

Junwen Tang, Mingyao Cui, Shenheng Xu, *Member, IEEE*, Linglong Dai, *Fellow, IEEE*, Fan Yang, *Fellow, IEEE*, and Maokun Li, *Senior Member, IEEE*

Abstract

Reconfigurable intelligent surface (RIS) has been widely considered as a key technique to improve spectral efficiency for 6G communications. Compared with most existing research that only focuses on the reflective RIS, the design and prototyping of a novel transmissive RIS are presented in this paper, and its enhancement to the RIS-aided communication system is experimentally demonstrated. The 2-bit transmissive RIS element utilizes the penetration structure, which combines a 1-bit current reversible dipole and a 90° digital phase shifter based on a quadrature hybrid coupler. A transmissive RIS prototype with 16×16 elements is designed, fabricated, and measured to verify the proposed design. The measured phase shift and insertion loss of the RIS element validate the 2-bit phase modulation capability. Being illuminated by a horn feed, the prototype achieves a maximum broadside gain of 22.0 dBi at 27 GHz, and the two-dimensional beamforming capability with scan angles up to $\pm 60^\circ$ is validated. The experimental results of the RIS-aided communication system verify that by introducing the extra gain and beam steering capability, the transmissive RIS is able to achieve a higher data rate, reduce the transmit power, improve the transmission capability through obstacles, and dynamically adapt to the signal propagation direction.

Index Terms

Transmissive RIS, 2 bit phase shifter, prototyping

Part of this work has been accepted by 2020 IEEE International Symposium on Antennas and Propagation and North American Radio Science Meeting [1].

All the authors are with the Department of Electronic Engineering, Tsinghua University, Beijing 100084, China (e-mails: tjw17@mails.tsinghua.edu.cn; cmy20@mails.tsinghua.edu.cn; {shxu, daill, fan_yang, maokunli}@tsinghua.edu.cn).

I. INTRODUCTION

With the explosive growth of the emerging new applications, such as holographic video and meta-verse, 6G is expected to achieve a $10\times$ increase in spectral efficiency compared to 5G [2], [3]. To realize this goal, the reconfigurable intelligent surface (RIS) has become an essential candidate [4]. By adjusting the phase and amplitude responses to an incident electromagnetic wave, RIS can achieve dynamic beamforming to enhance the spectral efficiency and overcome blockage [5].

Nevertheless, existing research contributions mainly consider the employment of reflective RIS [6]–[8], which may result in coverage holes in a cell. Specifically, for reflective RIS, the base station and user need to be located on the same side of the RIS, which brings extra geographical constraints on the physical topology [9]. For instance, reflective RIS is difficult to assist communication between a transmitter outside a vehicle and a receiver inside it. To cope with this problem, transmissive RIS has been recently proposed [10]. Rather than being reflected, signals can transmit through a transmissive RIS to form directional beams. In this way, transmissive RIS can potentially fill in the coverage holes of reflective RIS.

The phase reconfigurability is the most essential capability for a transmissive RIS. Solid-state electronic devices are commonly integrated in each constituent RIS element to dynamically control its phase response. Continuous phase shifts can be realized using analog-type devices like varactor diodes [10]–[17]. The phase shift range usually exceeds 360° so that the phase errors are negligible. However, the transmissive RIS has a very high transmission insertion loss, which can be up to 5.7 dB [13]. As a consequence, the aperture efficiency of the RIS is considerably reduced. At high frequencies, switch-type devices are widely used to produce discrete phase shifts, including PIN diodes, RF MEMS switches, and etc [13]–[17]. Most existing designs focus on 1-bit phase reconfigurability, where the design and fabrication difficulties are manageable [18]–[26]. For example, a classic design of an O-slot patch loaded with two PIN diodes was developed in [18] to achieve a stable 180° phase shift in a large bandwidth using the current reversal mechanism. The minimum measured insertion loss is 1.7/1.9 dB at 9.8 GHz. Several other attempts were made to obtain a 2-bit phase resolution [27], [28]. Specifically, a monolithically fabricated 2-bit prototype using MEMS switches [27] was able to produce 4 phase states, but the measured insertion loss is 4.2–9.2 dB at Ka band. A compact 2-bit element using a modified O-slot patch [28] was designed, fabricated and measured. The measured insertion

loss is 1.5–2.3 dB at 29.0 GHz, and the measured 3-dB transmission bandwidth is 10.1–12.1% for four phase states.

The phase quantization errors associated with discrete phase shifts inevitably introduce performance degradation [29]–[31]. It is observed that the 1-bit element designs suffer from 3–4 dB insertion loss attributed to the coarse phase resolution, which results in a low aperture efficiency. The sidelobe levels are significantly higher, sometimes even causing unwanted grating lobes. By contrast, 2-bit designs are considered a well-balanced choice between the element performance and the design complexity. The phase quantization loss can be greatly reduced to less than 1 dB, and the sidelobe envelop can be significantly improved as well.

Nonetheless, there are only a few 2-bit designs in the literature. One of the important reasons is that, compared to 1-bit designs, more transition structures, electronic devices and DC/RF biasing circuits are needed to achieve four stable phase states. The conventional design approach solely relies on the two-dimensional unit-cell footprint because of the printed-circuit board (PCB) fabrication process. It becomes extremely challenging to lay out a variety of constituent element parts in a greatly limited sub-wavelength array grid. Consequently, more numbers of stacked layers are used, which results in the higher fabrication complexity and cost. To the best of our knowledge, the design, fabrication, and measurement of the 2-bit transmissive RIS have not been well studied.

In this paper, the 2.5-D penetration structure [32] is exploited to make the best of the longitudinal space in the propagation direction to develop the 2-bit transmissive RIS. Specifically, our contributions are summarized below.

- Firstly, a 90° digital phase shifter with two PIN diodes based on a quadrature hybrid coupler [33] is proposed and realized. Combined with a 1-bit current reversible dipole, 2-bit phase resolution is achieved at the millimeter wave (mmWave) band. In addition to some preliminary results reported in the authors' conference paper [1], the 2-bit RIS element is further optimized and more detailed analysis is presented in this journal paper.
- Furthermore, a prototype with 16×16 RIS elements and a logic circuit control board is fabricated and measured. The measured results show that the prototype can achieve a maximum broadside gain of 22.0 dBi at 27 GHz, with the corresponding aperture efficiency of 25.3%. Moreover, the measured radiation performances for scan angles are presented as well, demonstrating the beamsteering capability in a large angle up to 60° .
- Finally, a transmissive RIS-aided mmWave wireless communication prototype is developed

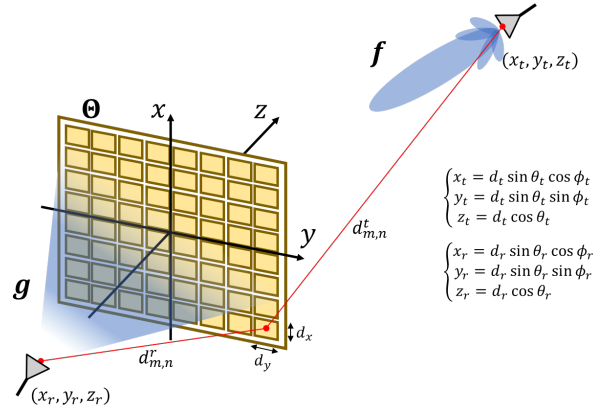


Fig. 1. System model of transmissive RIS-aided communication systems.

to demonstrate the performance of the fabricated 2-bit transmissive RIS. The experimental results verify that the 2-bit transmissive RIS can achieve a higher data rate, reduce the transmit power, improve the transmission capability through obstacles, and dynamically adapt to the signal propagation direction.

Organization: The remainder of this paper is organized as follows. The communication model of transmissive RIS is introduced in Section II. Then, in Section III, we describe the structure, biasing circuits, and simulated performance of the element of the designed transmissive RIS. Section IV provides the experimental results for the 16×16 elements RIS prototype in the microwave anechoic chamber. A transmissive RIS-aided wireless communication prototype is set up to further measure the performance of the proposed RIS in Section V. Finally in Section VI, conclusions are drawn.

II. SYSTEM MODEL

In this section, we describe the system model of the transmissive RIS-aided communication system.

A. System Model

We consider that the transmitter (Tx) employs a horn antenna to communicate with a single-antenna receiver (Rx), where an N-element transmissive RIS is used for enhancing the signal power. As shown in Fig. 1, the RIS is a uniformly planar array (UPA) placed in the x-y plane, and its geometric center is located at the origin of the coordinate system. Let N_x denote the number of antennas on the row and N_y denote the number of antennas on the column, with

$N = N_x N_y$. The antenna spacing along the x axis and y axis are d_x and d_y respectively, which are usually half of the wavelength. The coordinates of the Tx and Rx are (x_t, y_t, z_t) and (x_r, y_r, z_r) . The coordinate of the (m, n) -th antenna in the m -th row and n -th column of the RIS is $(\delta_m d_x, \delta_n d_y, 0)$, where $\delta_m = m - (N_x - 1)/2$ and $\delta_n = n - (N_y - 1)/2$ with $m \in \{0, 1, \dots, N_x - 1\}$ and $n \in \{0, 1, \dots, N_y - 1\}$. We use the symbols d_t , θ_t , and ϕ_t to denote the distance, the azimuth angle, and the elevation angle between the center of the RIS and the Tx. The relationship between (x_t, y_t, z_t) and (d_t, θ_t, ϕ_t) is shown in Fig. 1. Similarly, we use the symbols d_r , θ_r , and ϕ_r to denote the distance, the azimuth angle, and the elevation angle between the center of the RIS and the Rx, where the relationship between (x_r, y_r, z_r) and (d_r, θ_r, ϕ_r) is shown in Fig. 1 as well.

We denote $\mathbf{f} \in \mathbb{C}^{N \times 1}$ as the Tx-RIS channel, and denote $\mathbf{g} \in \mathbb{C}^{N \times 1}$ as the RIS-Rx channel. Since this paper aims to evaluate the function of the transmissive RIS, the direct link between the Tx and Rx is ignored in this paper. Denote $[\mathbf{g}]_{m,n}$ and $[\mathbf{f}]_{m,n}$ as the channel from the (m, n) -th antenna of the RIS to the Rx and Tx, respectively. Then, the free space channel model is adopted to represent $[\mathbf{g}]_{m,n}$ and $[\mathbf{f}]_{m,n}$ as [4]

$$[\mathbf{g}]_{m,n} = \sqrt{\frac{\lambda G_g F_g(\theta_r, \phi_r)}{4\pi}} \frac{e^{-j\frac{2\pi}{\lambda} d_{m,n}^r}}{d_{m,n}^r}, \quad (1)$$

$$[\mathbf{f}]_{m,n} = \sqrt{\frac{\lambda G_f F_f(\theta_t, \phi_t)}{4\pi}} \frac{e^{-j\frac{2\pi}{\lambda} d_{m,n}^t}}{d_{m,n}^t}, \quad (2)$$

where λ represents the wavelength, $d_{m,n}^r$ and $d_{m,n}^t$ denote the distance from the (m, n) -th antenna of the RIS to the Rx and Tx, respectively. Moreover, G_g and $F_g(\theta_r, \phi_r)$ denote the antenna gain and the normalized power radiation pattern of the side of RIS facing the receiver, while G_f and $F_f(\theta_t, \phi_t)$ correspond to those of the side of RIS facing the transmitter [4].

Let s denote the transmitted symbol with $\|s\|_2 = 1$. We use symbols G_t , F_t , P_t , G_r , F_r to represent the transmitter antenna gain, the transmit power, the normalized radiation power of the transmitter, the receiver antenna gain, and the normalized radiation power of the receiver. Then the noiseless received signal by the RX can be modeled as [4]

$$\begin{aligned} y &= \sqrt{P_t G F} \sum_{m=0}^{N_x-1} \sum_{n=0}^{N_y-1} [\mathbf{g}]_{m,n} [\mathbf{f}]_{m,n} \Gamma_{m,n} e^{j\phi_{m,n}} s, \\ &= \frac{\sqrt{P_t G F \lambda}}{4\pi} \sum_{m=0}^{N_x-1} \sum_{n=0}^{N_y-1} \frac{\Gamma_{m,n}}{d_{m,n}^t d_{m,n}^r} e^{j\left(\phi_{m,n} - \frac{d_{m,n}^t + d_{m,n}^r}{\lambda}\right)} s, \end{aligned} \quad (3)$$

where $\Gamma_{m,n} \in [0, 1]$ is transmission loss of the (m, n) -th antenna of the RIS, $\phi_{m,n} \in [0, 2\pi]$ denotes the phase shift of the (m, n) -th antenna of the RIS, $G = G_t G_f G_g G_r$, and $F = F_t F_f(\theta_r, \phi_r) F_g(\theta_r, \phi_r) F_r$.

B. Beamforming for the Transmissive RIS

For the desired receiver, the transmissive RIS is designed for maximizing the received signal energy through beamforming. The noiseless received signal energy can be presented as

$$P_r = \frac{P_t G F \lambda^2}{16\pi^2} \left| \sum_{m=0}^{N_x-1} \sum_{n=0}^{N_y-1} \frac{\Gamma_{m,n}}{d_{m,n}^t d_{m,n}^r} e^{j\left(\phi_{m,n} - \frac{d_{m,n}^t + d_{m,n}^r}{\lambda}\right)} \right|^2. \quad (4)$$

To maximize P_r , it is obvious that the optimal $\phi_{m,n}$ is

$$\bar{\phi}_{m,n} = \text{mod} \left(C + \frac{d_{m,n}^t + d_{m,n}^r}{\lambda}, 2\pi \right). \quad (5)$$

Here, C is an arbitrary constant. From (5), the phase shift $\phi_{m,n}$ can be obtained according to $d_{m,n}^t$ and $d_{m,n}^r$. In our practical employment, the RIS is deployed nearby the Rx and far away from the Tx. That is to say, the Rx is within the near-field range of the RIS, while the Tx is within the far-field range of the RIS. Based on this assumption, the distance $d_{m,n}^r$ can be derived according to the spherical wave model as

$$d_{m,n}^r = \sqrt{(x_r - \delta_m d_x)^2 + (y_r - \delta_n d_y)^2 + z_r^2}, \quad (6)$$

while the distance $d_{m,n}^t$ can be simplified by the planar wave model as

$$\begin{aligned} d_{m,n}^t &= \sqrt{(x_t - \delta_m d_x)^2 + (y_t - \delta_n d_y)^2 + z_t^2} \\ &\approx r_t - \delta_m d_x \sin \theta_t \cos \phi_t - \delta_n d_y \sin \theta_t \sin \phi_t. \end{aligned} \quad (7)$$

Therefore, the optimal solution to $\phi_{m,n}$ can be obtained accordingly. Then, for practical implementation of RIS, the limited resolution of the phase shift has to be considered. If there are b bits for quantized phase shifter, then the feasible set of phase shift is

$$\Phi_b = \left\{ 0, \frac{1}{2^{b-1}}\pi, \dots, \frac{2^b - 1}{2^{b-1}}\pi \right\}. \quad (8)$$

Finally, the practical phased shift on a RIS element is given by

$$\tilde{\phi}_{m,n} = \arg \min_{\phi \in \Phi_b} |\phi - \bar{\phi}_{m,n}|. \quad (9)$$

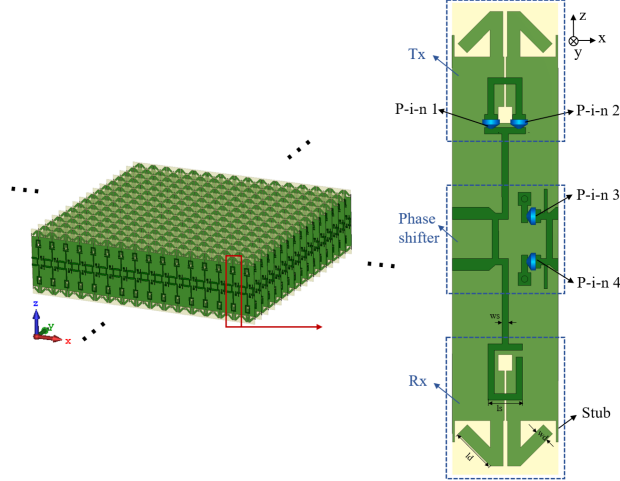


Fig. 2. Proposed 2.5-D structure of the transmissive RIS for mmWave communications.

In our system, we design a transmissive RIS with $b = 2$ bits. Notice that the transmission model and the phase shift design mathematically have no difference with the reflective RIS-aided communication system. Nevertheless, the application scenarios and implementation and of them are quite different. For instance, a transmissive RIS can be deployed on a vehicle window to enhance communication between inside and outside the vehicle. In the following sections, we will elaborate on the proposed transmissive RIS design in our communication system.

III. PROPOSED RIS ELEMENT DESIGN

We describe the proposed transmissive RIS element in this section, including element design, 90° phase shifter exploited in the element, biasing circuits, and element performance in simulation.

A. Element Design

Fig. 2 illustrates the proposed 2.5-D structure of the 2-bit transmissive RIS. Each RIS element consists of a number of one-dimensional subarrays aligned in parallel. The constituent element utilizes the penetration structure, which is composed of a RIS-side Rx and a RIS-side Tx to receive and transmit the RF signals impinging on the RIS, respectively, and a microstrip transmission line to convey the signal through the RIS aperture. Instead of laying them out in the aperture plane, two vertical dipoles [34] are employed and arranged along the propagation direction to circumvent the space constraint imposed by the unit cell footprint. The slightly

TABLE I
SIMULATED PERFORMANCE OF THE 2-BIT RIS ELEMENT

State	Element loss @26.5 GHz	Phase shift @26.5 GHz	3-dB trans. bandwidth
1 (state-0°)	1.1 dB	-141.2°	23.6-28.9 GHz (20.1%)
2 (state-90°)	1.3 dB	-56.8°	24.8-28.6 GHz (14.2%)
3 (state-180°)	1.1 dB	34.9°	23.5-28.6 GHz (19.6%)
4 (state-270°)	1.5 dB	129.0°	24.6-29.0 GHz (16.4%)

extended longitudinal space easily accommodates a 90° digital phase shifter between the RIS-side Rx and the RIS-side Tx. Combined with the 1-bit current reversible dipole, the 2-bit transmissive RIS element can be readily realized.

The 2.5-D structure slightly increases the aperture profile by 1/2 wavelengths, but it is still much smaller compared with the aperture size. Especially at mmWave frequencies, the aperture profile is merely a couple of centimeters and will not considerably undermine the low profile and conformal features of the RIS. Each subarray can be easily fabricated on a single layer of substrate, thus avoiding the complicated multilayer PCB process and lowering the overall cost. It is also a remarkable fact that the // -type 2.5-D structure can be further developed into a # -type or a Δ -type formation where two or three sets of subarrays can be arranged in the same aperture, so that the 2.5-D unit cell space can be more fully exploited for more constituent element parts. Hence, more advanced features such as dual-polar or dual-band designs can be accomplished.

The linearly incident wave propagating along the z axis is received by the passive RIS-side Rx composed of a vertical dipole. Then, the received signal is converted into a guided wave and conveyed along the microstrip transmission line. The phase shifter structure based on the quadrature hybrid coupler is employed. Instead of the varactor diodes used in the analog phase shifter design [33], it is terminated with reflection-type loads composed of two p-i-n diodes (model MADP-000907-14020) to provide a 0°/90° digital phase shift. The two loaded p-i-n diodes are always tuned at the same ON- or OFF-states, resulting in a 90° phase shift. The RIS-side Tx is similar to the RIS-side Rx, but the vertical dipole structure [34] is modified to integrate two p-i-n diodes (MADP-000907-14020) that are symmetrically placed in the feeding microstrip line. They are alternatively turned ON or OFF so that the excitation current flows

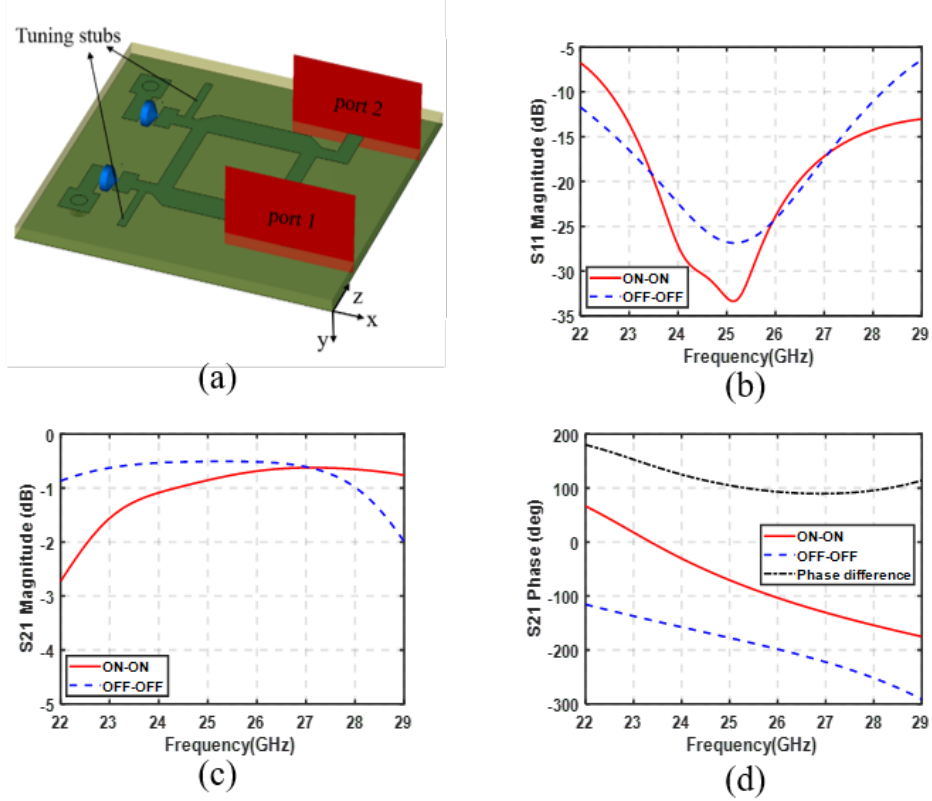


Fig. 3. Proposed 90° digital phase shifter based on a quadrature hybrid coupler: (a) the illustrative structure; (b) simulated reflection magnitude, (c) transmission magnitude, and (d) transmission phase.

in opposite directions. Consequently, the reversible current flow produces a stable 180° phase shift without significantly affecting magnitude response. Finally, the RIS-side Tx re-radiates the guided wave into the free space with four stable phase states of 0°/90°/180°/270°, and hence, the 2-bit phase resolution is obtained.

The frequency of the designed transmissive RIS element is 26.5 GHz, and the unit cell size is $4.9 \times 4.9 \text{ mm}^2$. The proposed 2-bit element is printed on a single layer of Taconic TLX-8 substrate ($\epsilon_r = 2.55$, $\tan \delta = 0.0019$, $h = 0.254 \text{ mm}$). The microstrip line and the 90° digital phase shifter are on the top of the substrate, while the vertical dipoles and the ground plane are arranged on the bottom of the substrate. The total profile of the element is 21.8 mm, corresponding to 1.9λ at the design frequency. The following geometrical parameters are optimized after a comprehensive parametric study: $l_d = 2.1 \text{ mm}$, $w_d = 0.6 \text{ mm}$, $l_s = 1.6 \text{ mm}$, $w_s = 0.3 \text{ mm}$.

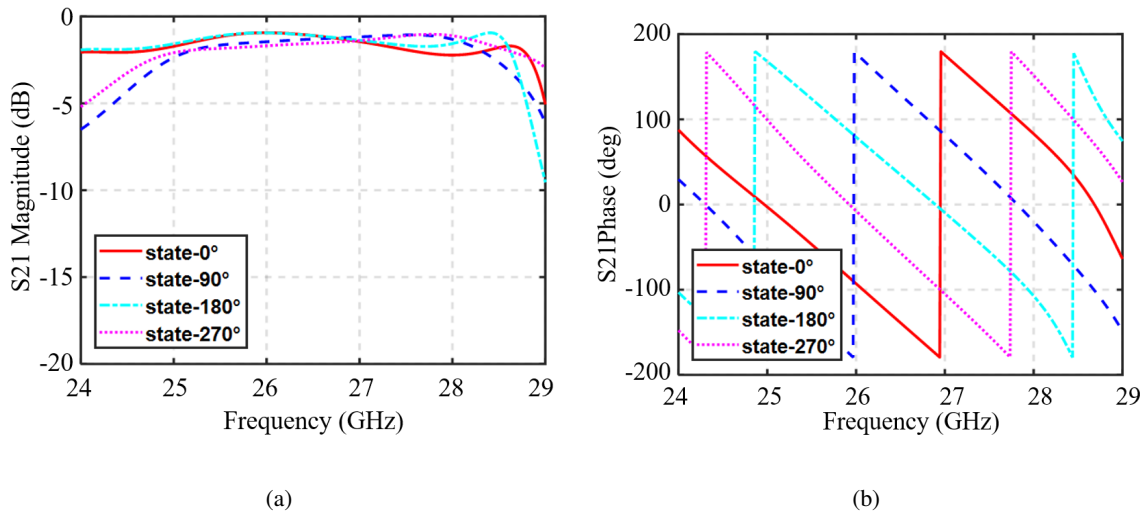


Fig. 4. Simulated transmission (a) magnitude and (b) phase of the proposed 2-bit RIS element.

B. 90° Digital Phase Shifter

The proposed 90° digital phase shifter integrated in the 2-bit transmissive RIS element is designed to provide $0^\circ/90^\circ$ phase switching, as shown in Fig. 3 (a). It is a reflection-type phase shifter based on the quadrature coupler terminated with two reflective loads, which are composed of p-i-n diodes and short-circuited stubs. The realization of 90° phase shift is by tuning the two p-i-n diodes to work at ON-ON or OFF-OFF state, respectively. Two tuning stubs are introduced to maintain a stable desired phase shift by tuning their lengths. The digital phase shifter is modeled and simulated with a periodic boundary condition and a wave-port excitation. As can be observed from the simulation results plotted in Fig. 3 (b), a 10-dB return loss bandwidth of 22% (22.6-28.2 GHz) is achieved. Good impedance matching performance minimizes the insertion loss to less than 1 dB within the frequency band from 24.2 to 28.0 GHz. Meanwhile, from the curves plotted in Fig. 3 (d), we can find that the phase difference is close to 90° in a wide frequency band. We can conclude that the phase shifter is capable of generating desired 90° phase shift by electrically adjusting the two p-i-n diodes, thus achieving the $0^\circ/90^\circ$ digital phase switching capability with the low insertion loss.

C. Performance of the designed Transmissive RIS Element

We simulate the proposed 2-bit RIS element with a periodic boundary condition to mimic an infinite array environment and the mutual coupling effect is also considered. The element is simulated. The simulated element performances under normal incidence for the four working

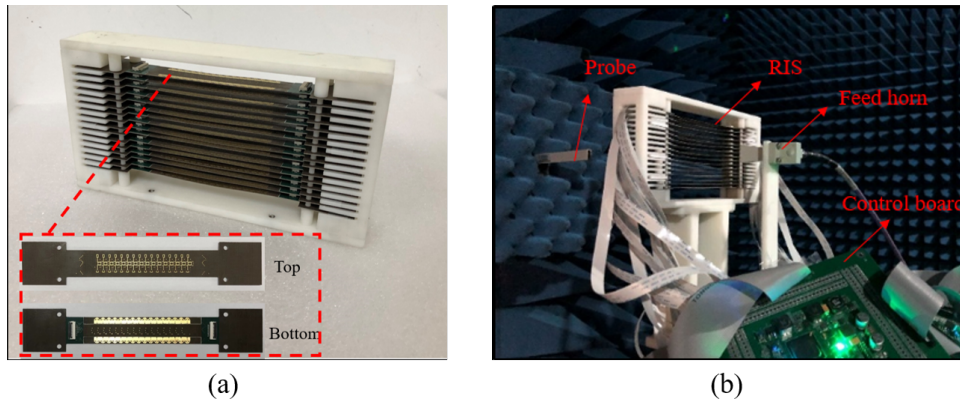


Fig. 5. Photography of (a) the fabricated transmissive RIS prototype, (b) the measurement setup in the microwave anechoic chamber.

states are plotted in Fig. 4. The transmission magnitude responses at 26.5 GHz are summarized in Table I. It can be seen that the average transmission insertion loss of the four states is around 1.3 dB. Moreover, the insertion losses are maintained below 3 dB ranging from 24.8 to 28.6 GHz, corresponding to the 3-dB transmission bandwidth of 14.2%. The phase curves of the four states are roughly parallel with around 90° phase difference in the operating frequency band. Hence, by switching the p-i-n diodes alternatively, the RIS element successfully achieves 2-bit phase tuning capability.

IV. RIS DESIGN, FABRICATION, AND MEASUREMENT

In this section, a transmissive RIS prototype composed of 16×16 proposed elements is designed, fabricated, and measured to experimentally validate the performance of the proposed RIS element.

The photographs of the fabricated RIS prototype and the measurement setup in the microwave anechoic chamber are presented in Fig. 5. Taking advantage of the PCB technology, the RIS is easy to fabricate. The RIS is space-fed by a linearly polarized horn. The effective aperture size of the RIS prototype is $78.4 \times 78.4 \text{ mm}^2$. The feeding horn illuminates the array at an optimized distance of 50 mm. To achieve the goal of phase reconfigurability, each element of the array needs to be controlled independently. There are 512 biasing lines since each element has two biasing lines to apply DC voltages to four p-i-n diodes. Two logic circuit controlling boards are attached to supply independent DC voltages of 512 channels, and they are connected to the biasing lines through several connectors.

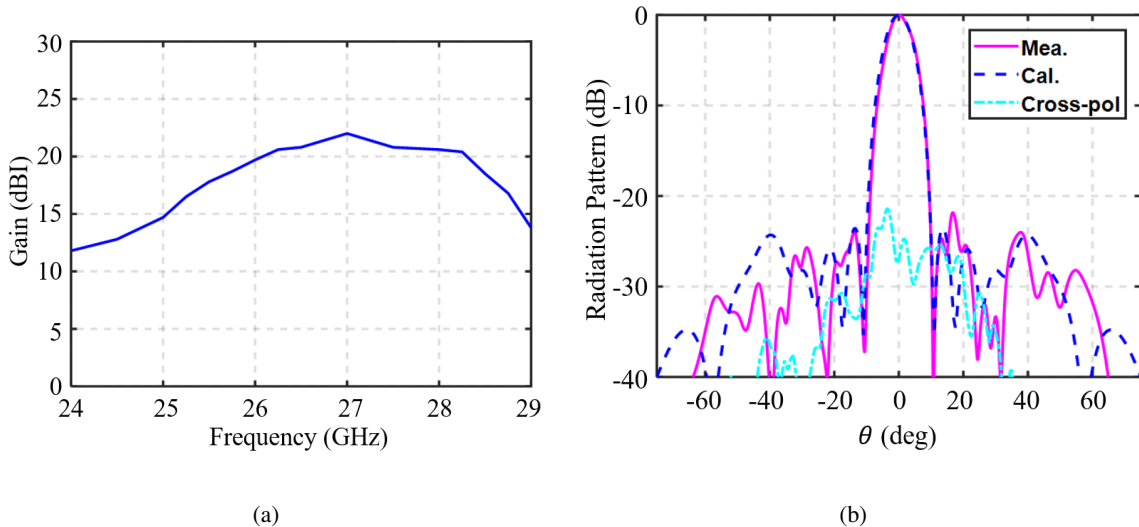


Fig. 6. Performance of the broadside beam: (a) measured gain bandwidth, (b) calculated and measured normalized radiation patterns at 27.0 GHz.

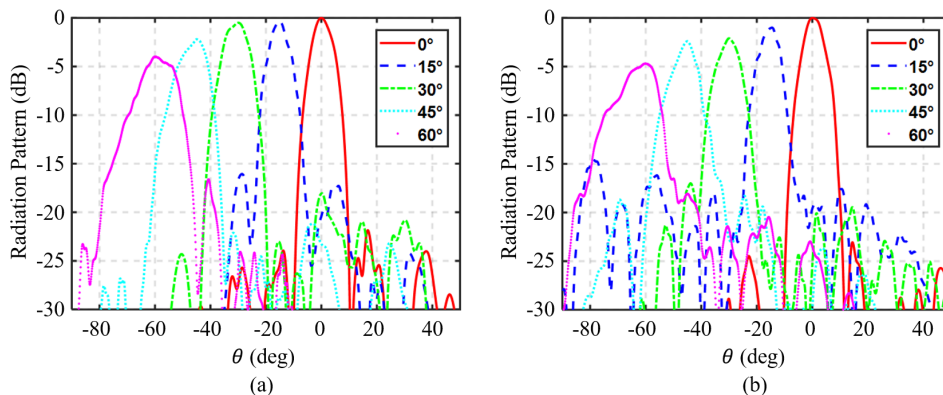


Fig. 7. Measured radiation patterns of scanned beams at 27.0 GHz in (a) E-plane, (b) H-plane.

We measure the fabricated prototype in a planar near-field anechoic chamber. From the measured performance of the broadside beam depicted in Fig. 6, a peak gain of 22.0 dBi is obtained at 27.0 GHz, which is 9.3 dB higher than that of the feeding horn. The corresponding aperture efficiency is 25.3%. The slight frequency shift to higher frequencies is mainly attributed to the tolerance in fabrication and the supporting structure. The measured radiation pattern is in good agreement with the theoretical prediction based on the array theory. The measured sidelobe level is below -22 dB, remarkably lower than that of the 1-bit designs, which is mainly attributed to the finer phase resolution of the 2-bit RIS. The measured cross-polarization level is -21.3 dB.

TABLE II
PERFORMANCE COMPARISON WITH OTHER TRANSMISSIVE RIS DESIGNS

Ref.	Freq. [GHz]	Tunable device	Phase resolution	Gain [dBi]	Aper. eff. [%]
[18]	9.8	p-i-n	1-bit	22.7	15.4
[26]	34.8	MEMS	2-bit	9.2	6.2
[27]	29	p-i-n	2-bit	19.8	15.9
Our work	27	p-i-n	2-bit	22.0	25.3

The radiation behaviors of the scanned beams are measured as well to experimentally verify the dynamic beam scanning capability of the transmissive RIS in two-dimensional space. By controlling the phase of each RIS element, the transmitted focused beam can be formed by the RIS in the given direction. As shown in Fig. 7, the measured scanned beams in the angular region from 0° to -60° show accurate beam pointing and well-defined patterns in both E-plane and H-plane. Note that the beams in the opposite angular region are omitted due to the symmetry. The measured 60° scan gain losses are 4.0 dB and 5.0 dB in two principal planes, respectively. Table II compares the performance of the proposed 2-bit RIS with other RIS designs published in literature. It is evident that this work achieves the highest aperture efficiency.

V. TRANSMISSIVE RIS-AIDED WIRELESS COMMUNICATION PROTOTYPE

In this section, a transmissive RIS-aided wireless communication prototype is set up to further measure the performance of the designed transmissive RIS in practical communication scenarios.

A. Measurement Setup

As illustrated in Fig. 8, we carry out the experiment in an office environment. The prototype is composed of the transmitter side, the RIS, and the receiver side. Both the receiver and the transmitter utilize the software-defined radio (SDR) platform, composed of the PXI hardware architecture and the LabVIEW system design software, to realize transmission at the mmWave band.

The transmitter consists of the transmitter host, the FPGA, the ADC module, the mmWave upconverter, and a horn antenna. The transmitter host controls the system parameters, including

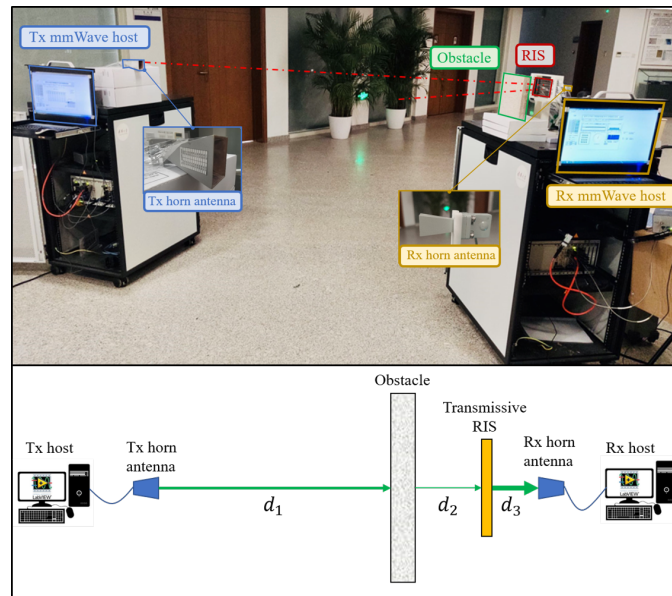


Fig. 8. Transmissive RIS-aided wireless communication prototype.

TABLE III
SYSTEM PARAMETERS

Parameters	Value	Parameters	Value
Carrier frequency	27.0 GHz	Antenna gain	Tx 22.7
System bandwidth	800 MHz		Rx 9.2
Waveform	CP-OFDM	Trans.	Array gain 19.8
FFT size	2048		Frequency 22.0
Carrier spacing	75 KHz	RIS	Phase resolution 2 bit
ADC/DAC resolution	14 bit		Array size 16×16
		Tx/Rx height 1.5 m	
Modulation	16-QAM	d_1	2.4 m
Coding	Turbo	d_2	0.2 m
Code rate	1/2	d_3	0.05 m

modulations, the transmit power, the central frequency, and so on. A high-speed bitstream is first delivered by the host to the FPGA module. The FPGA module realizes complex signal processing, including channel coding, constellation mapping, OFDM modulation, and etc. After that, the signals are sequentially processed by the ADC and the mmWave upconverter to form mmWave analog signals suitable for transmission in wireless channels.

The transmissive RIS has 256 2-bit elements. It receives the signals from the transmitter, tunes the phase of received signals, and then directionally transmits them towards the receiver. Moreover, for validating that a transmissive RIS is able to overcome obstacles, we can also place an obstacle, such as a piece of marble, between the RIS and the base station.

Similar to the transmitter, the receiver is composed of the receiver host, the FPGA, a DAC module, a mmWave down converter, and a horn antenna. At the receiver side, the Rx horn antenna first receives the signal and transforms them the digital domain by the mmWave down converter and the DAC module. Then, the FPGA module is responsible for recovering the bitstream by channel estimation, OFDM demodulation, decoding, CRC check and etc. Moreover, according to the results of the CRC check, the host obtains the block error rate and calculates the data rate. Finally, the received constellation and the data rate are illustrated on the screen of the host.

In Table III, the detailed settings of our mmWave platform are provided. We consider a downlink communication scenario. The bandwidth is 800 MHz and the carrier frequency is 27.0 GHz. The horn antenna of the transmitter, the transmissive RIS, and the horn antenna of the receiver are on the same height of 1.5 m and are all horizontally polarized. A piece of marble with thickness of 0.03 m is employed to mimic the obstacle. Let d_1 , d_2 , and d_3 denote the the distance between the Tx antenna and the obstacle, the distance between the obstacle and the RIS, the distance between the RIS and the Rx antenna. They are set as $d_1 = 2.4$ m, $d_2 = 0.2$ m, and $d_3 = 0.05$ m, respectively. The fabricated transmissive RIS works at 27.0 GHz with an additional 9.3 dB array gain when being illuminated by the Rx horn antenna. The azimuth angle and the elevation angle from the RIS center to the Tx/Rx are all zero, i.e., $\theta_t = \theta_r = \phi_t = \phi_r = 0^\circ$ as shown in Fig. 1. We verify the performance of this RIS in terms of array gain and data rate.

B. Array Gain Performance Assessment

To evaluate the array gain, we remove the obstacle and assess the system performance with or without the transmissive RIS. The experiment results are presented in Table IV. Specifically,

TABLE IV
ARRAY GAIN PERFORMANCE

With or without RIS	Transmit power	Data rate
×	13.6 dBm	1024 Mbps
✓	5.4 dBm	1121 Mbps

TABLE V
DATA RATE PERFORMANCE

With or without RIS	With or without obstacle	Azimuth angle	Data rate
×	×	0°	1024 Mbps
✓	×	0°	1683 Mbps
×	✓	0°	0 Mbps
✓	✓	0°	1683 Mbps

without the transmissive RIS, when the transmit power reaches 13.6 dBm, the data rate can reach 1024 Mbps. By contrast, to achieve a similar transmission rate of 1121 Mbps, only 5.4 dBm transmit power is required with the help of transmissive RIS. It is obvious that the transmit power is reduced by 8.2 dB. As we measured in the anechoic chamber, the RIS can provide a 9.3 dB array gain, which is consistent with the transmit power reduction measured by our prototype. Therefore, it is obtained that the transmissive RIS-aided communication prototype can reduce the transmit power by the magnitude close to the array gain provided by the RIS, while maintaining the similar communication performance.

C. Data Rate Assessment

To further validate that the fabricated transmissive RIS is able to overcome obstacles, we also introduce a piece of marble into the system to evaluate the data rate performance. Specifically, depending on whether the obstacle and/or the RIS exist, there are in total four communication scenarios. The transmit power is fixed to 13.6 dBm. The experiment results are tabulated in Table V. Two conclusions can be derived accordingly. One is that the fabricated RIS is able to improve the transmission data rate. When the obstacle is removed, the introduction of the

TABLE VI
BEAM STEERING EVALUATION

With or without RIS	With or without obstacle	Azimuth angle	Data rate
×	×	30°	450 Mbps
✓	×	30°	1683 Mbps
×	✓	30°	0 Mbps
✓	✓	30°	1683 Mbps

transmissive RIS increases the data rate from 1024 Mbps to 1683 Mbps. It is worth mentioning that 1683 Mbps is the highest data rate that the communication prototype can support with 16-QAM modulation. The other is that the transmissive RIS is able to overcome obstacles because of the additional array gain it provides. Specifically, when the direct Tx-Rx link is blocked by the marble, data transmission is completely interrupted without the help of transmissive RIS. By contrast, the introduction of the transmissive RIS re-establishes the communication link and achieves the highest 1683 Mbps. This is because that the array gain provided by the RIS is higher than the attenuation of the obstacle.

D. Beam Steering Assessment

Finally, the beam steering ability of the fabricated transmissive array is validated in this subsection. Compared to the communication settings in previous experiments, the transmit power is fixed to 13.6 dBm and the azimuth angle from the transmissive RIS to the transmitter is $\theta_t = 30^\circ$. The other settings are the same. The experiment results are shown in Table VI. Without the assistance of transmissive RIS, the data rate is reduced from 1024 Mbps to 450 Mbps due to the misalignment between the Tx and Rx horns. By introducing the transmissive RIS and scanning the beam it forms to the 30° direction, the maximum 1683 Mbps data rate is achieved. As a result, we can conclude that the transmissive RIS is able to dynamically steer its beam to adapt to the variation of the incident angle of the signal. Similar to the experiment in the previous subsection, the obstacle is again introduced into the communication prototype. The experiment results validate that the transmissive RIS is able to improve the data rate and overcome obstacles at an oblique incident angle $\theta_i = 30^\circ$.

VI. CONCLUSION

The transmissive RIS has a promising prospect in 6G communications to provide enhanced signal coverage in various communication scenarios. Compared to the reflective RIS, the research and experimental demonstration of the transmissive RIS and the transmissive RIS-aided communication system are considerably fewer. This work proposes a novel 2-bit transmissive RIS design with a 90° digital phase shifter and a 1-bit vertical current reversible dipole. The 2-bit phase controlling capability is achieved and measured. Experimental results show the transmissive RIS prototype with 16×16 elements can provide a broadside gain of 22.0 dBi at 27.0 GHz. Moreover, a transmissive RIS-aided communication prototype is set up, and the system performances for three representative scenarios are measured. It is experimentally demonstrated that the transmissive RIS is able to achieve higher data rate, reduce the transmit power, improve the transmission capability through obstacles, and dynamically adapt to the signal propagation direction.

REFERENCES

- [1] J. Tang, S. Xu, and F. Yang, "Design of a 2.5-D 2-bit reconfigurable transmitarray element for 5G mmWave applications," in *Proc. 2020 IEEE Int. Symp. Antennas and Propag.*, 2020, pp. 631–632.
- [2] F. E. Idachaba, "5G networks: Open network architecture and densification strategies for beyond 1000x network capacity increase," in *proc. Future Technol. Conf.*, 2016, pp. 1265–1269.
- [3] T. S. Rappaport, Y. Xing, O. Kanhere, S. Ju, A. Madanayake, S. Mandal, A. Alkhateeb, and G. C. Trichopoulos, "Wireless communications and applications above 100 GHz: Opportunities and challenges for 6G and beyond," *IEEE Access*, vol. 7, pp. 78 729–78 757, Jun. 2019.
- [4] W. Tang, M. Z. Chen, X. Chen, J. Y. Dai, Y. Han, M. Di Renzo, Y. Zeng, S. Jin, Q. Cheng, and T. J. Cui, "Wireless communications with reconfigurable intelligent surface: Path loss modeling and experimental measurement," *IEEE Trans. Wireless Commun.*, vol. 20, no. 1, pp. 421–439, Jan. 2021.
- [5] P. Wang, J. Fang, X. Yuan, Z. Chen, and H. Li, "Intelligent reflecting surface-assisted millimeter wave communications: Joint active and passive precoding design," *IEEE Trans. Veh. Tech.*, vol. 69, no. 12, pp. 14 960–14 973, Dec. 2020.
- [6] C. Huang, A. Zappone, G. C. Alexandropoulos, M. Debbah, and C. Yuen, "Reconfigurable intelligent surfaces for energy efficiency in wireless communication," *IEEE Trans. Wireless Commun.*, vol. 18, no. 8, pp. 4157–4170, Aug. 2019.
- [7] L. Dai, B. Wang, M. Wang, X. Yang, J. Tan, S. Bi, S. Xu, F. Yang, Z. Chen, M. D. Renzo, C.-B. Chae, and L. Hanzo, "Reconfigurable intelligent surface-based wireless communications: Antenna design, prototyping, and experimental results," *IEEE Access*, vol. 8, pp. 45 913–45 923, 2020.
- [8] Z. Zhang and L. Dai, "A joint precoding framework for wideband reconfigurable intelligent surface-aided cell-free network," *IEEE Trans. Signal Process.*, vol. 69, pp. 4085–4101, Jun. 2021.
- [9] J. Xu, Y. Liu, X. Mu, and O. A. Dobre, "STAR-RISs: Simultaneous transmitting and reflecting reconfigurable intelligent surfaces," *IEEE Commun. Lett.*, vol. 25, no. 9, pp. 3134–3138, Sep. 2021.

- [10] “DOCOMO conducts world’s first successful trial of transparent dynamic metasurface,” 2020. [Online]. Available: www.nttdocomo.co.jp/english/info/mediacenter/pr/2020/011700.html
- [11] M. Sazegar, Y. Zheng, C. Kohler, H. Maune, M. Nikfalazar, J. R. Binder, and R. Jakoby, “Beam steering transmitarray using tunable frequency selective surface with integrated ferroelectric varactors,” *IEEE Trans. Antennas Propag.*, vol. 60, no. 12, Dec. 2012.
- [12] L. Boccia, I. Russo, G. Amendola, and G. Di Massa, “Multilayer antenna-filter antenna for beam-steering transmit-array applications,” *IEEE Trans. Microw. Theory Techn.*, vol. 60, no. 7, pp. 2287–2300, Jul. 2012.
- [13] J. Y. Lau and S. V. Hum, “Analysis and characterization of a multipole reconfigurable transmitarray element,” *IEEE Trans. Antennas Propag.*, vol. 59, no. 1, pp. 70–79, 2011.
- [14] W. Pan, C. Huang, X. Ma, and X. Luo, “An amplifying tunable transmitarray element,” *IEEE Antennas Wireless Propag. Lett.*, vol. 13, pp. 702–705, 2014.
- [15] J. Y. Lau and S. V. Hum, “Reconfigurable transmitarray design approaches for beamforming applications,” *IEEE Trans. Antennas Propag.*, vol. 60, no. 12, pp. 5679–5689, Dec. 2012.
- [16] C. Huang, W. Pan, X. Ma, B. Zhao, J. Cui, and X. Luo, “Using reconfigurable transmitarray to achieve beam-steering and polarization manipulation applications,” *IEEE Trans. Antennas Propag.*, vol. 63, no. 11, pp. 4801–4810, Nov. 2015.
- [17] M. Frank, F. Lurz, R. Weigel, and A. Koelpin, “Electronically reconfigurable 6×6 element transmitarray at K-Band based on unit cells with continuous phase range,” *IEEE Antennas Wireless Propag. Lett.*, vol. 18, pp. 796–800, 2019.
- [18] A. Clemente, L. Dussopt, R. Sauleau, P. Potier, and P. Pouliguen, “1-bit reconfigurable unit cell based on PIN diodes for transmit-array applications in X-band,” *IEEE Trans. Antennas Propag.*, vol. 60, no. 5, pp. 2260–2269, May 2012.
- [19] W. Pan, C. Huang, X. Ma, B. Jiang, and X. Luo, “A dual linearly polarized transmitarray element with 1-Bit phase resolution in X-band,” *IEEE Antennas Wireless Propag. Lett.*, vol. 14, pp. 167–170, 2015.
- [20] L. Di Palma, A. Clemente, L. Dussopt, R. Sauleau, P. Potier, and P. Pouliguen, “Circularly-polarized reconfigurable transmitarray in Ka-band with beam scanning and polarization switching capabilities,” *IEEE Trans. Antennas Propag.*, vol. 65, no. 2, pp. 529–540, Feb. 2017.
- [21] B. D. Nguyen and C. Pichot, “Unit-cell loaded with PIN diodes for 1-Bit linearly polarized reconfigurable transmitarrays,” *IEEE Antennas Wireless Propag. Lett.*, vol. 18, pp. 98–102, 2019.
- [22] M. Wang, S. Xu, F. Yang, and M. Li, “A 1-Bit bidirectional reconfigurable transmit-reflect-array using a single-layer slot element with PIN diodes,” *IEEE Trans. Antennas Propag.*, vol. 67, no. 9, pp. 6205–6210, Sep. 2019.
- [23] L. Di Palma, A. Clemente, L. Dussopt, R. Sauleau, P. Potier, and P. Pouliguen, “Experimental characterization of a circularly polarized 1 Bit unit cell for beam steerable transmitarrays at Ka-band,” *IEEE Trans. Antennas Propag.*, vol. 67, no. 2, pp. 1300–1305, Feb. 2019.
- [24] Y. Wang, S. Xu, F. Yang, and D. H. Werner, “1 Bit dual-linear polarized reconfigurable transmitarray antenna using asymmetric dipole elements with parasitic bypass dipoles,” *IEEE Trans. Antennas Propag.*, vol. 69, no. 2, pp. 1188–1192, Feb. 2021.
- [25] C.-W. Luo, G. Zhao, Y.-C. Jiao, G.-T. Chen, and Y.-D. Yan, “Wideband 1 bit reconfigurable transmitarray antenna based on polarization rotation element,” *IEEE Antennas Wireless Propag. Lett.*, vol. 20, pp. 798–802, 2021.
- [26] A. Clemente, L. Dussopt, R. Sauleau, P. Potier, and P. Pouliguen, “Wideband 400-element electronically reconfigurable transmitarray in X band,” *IEEE Trans. Antennas Propag.*, vol. 61, no. 10, pp. 5017–5027, Oct. 2013.
- [27] C.-C. Cheng, B. Lakshminarayanan, and A. Abbaspour-Tamijani, “A programmable lens-array antenna with monolithically integrated mems switches,” *IEEE Trans. Microw. Theory Techn.*, vol. 57, no. 8, Aug. 2009.
- [28] F. Diaby, A. Clemente, R. Sauleau, K. T. Pham, and L. Dussopt, “2 bit reconfigurable unit-cell and electronically steerable transmitarray at Ka -band,” *IEEE Trans. Antennas Propag.*, vol. 68, no. 6, pp. 5003–5008, 2020.

- [29] B. Wu, A. Sutinjo, M. E. Potter, and M. Okoniewski, "On the selection of the number of bits to control a dynamic digital MEMS reflectarray," *IEEE Antennas Wireless Propag. Lett.*, vol. 7, pp. 183–186, 2008.
- [30] H. Yang, F. Yang, S. Xu, M. Li, X. Cao, J. Gao, and Y. Zheng, "A study of phase quantization effects for reconfigurable reflectarray antennas," *IEEE Antennas Wireless Propag. Lett.*, vol. 16, pp. 302–305, 2017.
- [31] Q. Wu and R. Zhang, "Beamforming optimization for wireless network aided by intelligent reflecting surface with discrete phase shifts," *IEEE Trans. Commun.*, vol. 68, no. 3, pp. 1838–1851, Mar. 2020.
- [32] Y. Xiao, F. Yang, S. Xu, M. Li, K. Zhu, and H. Sun, "Design and implementation of a wideband 1-bit transmitarray based on a Yagi–Vivaldi unit cell," *IEEE Trans. Antennas Propag.*, vol. 69, no. 7, pp. 4229–4234, Jul. 2021.
- [33] T. Lambard, O. Lafond, M. Himdi, H. Jeuland, and S. Bolioli, "A novel analog 360° phase shifter design in Ku and Ka bands," in *Proc. 4th Euro. Conf. Antennas Propag. (EuCAP)*, 2010, pp. 1–4.
- [34] S. X. Ta, H. Choo, and I. Park, "Broadband printed-dipole antenna and its arrays for 5G applications," *IEEE Antennas Wireless Propag. Lett.*, vol. 16, pp. 2183–2186, 2017.